GI_Forum 2017, Issue 1
Page: 69 - 78
Full Paper
Corresponding Author:
stefan.kraxberger@stud.sbg.ac.at
DOI: 10.1553/giscience2017_01_s69

3D Electrical Resistivity Tomography in the Mondsee Catchment

Stefan Kraxberger, Damian Taferner and Hermann Klug
University of Salzburg, Austria

Abstract

Glacially formed slopes in the Mondsee catchment close to Koppl, Austria, expose high hydrological dynamics after intense rainfall events. We use Electrical Resistivity Tomography (ERT) to identify the subsurface geological structure relevant for springs causing surface runoff during storm events at times of fully saturated soils. To identify the horizontal and vertical distribution of subsurface structures, we use 26 parallel ERT profile lines with 6m spacing, and 4m electrode spacing, over a total length of 88m. After 3D inversion, the electrical resistivity values in the generated model comprise 10 to 1132 Ωm. Sections with resistivity values between 10 and 100 Ωm, classified as water-saturated material, dominate the uppermost 3m of the model. Highest resistivity (>200 Ωm) materials are classified as moraine material, which forms the steepest part of the slope covered by a coppice belt. Linear features with lowest resistivity values show congruencies with streams from runoff modelling and crop-out of springs. Finally, the model enables the identification of aquifers and aquicludes relevant for further 3D hydrological modelling.

Keywords:

subsurface modelling, hydrogeology, surface runoff

1 Introduction

In recent decades, the Mondsee catchment in Austria has been subject to extreme events (Klug & Oana, 2015) and is likely to be subject to further events in the future (Hofstätter et al., 2010). These events caused fully saturated soils, surface runoff, and flooding with related sediment transport (Swierczynski et al., 2012; Swierczynski et al., 2013). Because of surface runoff and sediment transport, nutrients like phosphorus are transported. This transport of nutrients is among the various parameters which repeatedly cause the Mondsee to fail to achieve a good ecological status according to the Water Framework Directive (Klug et al., 2015). To enable an 'automated geosynthesis' of environmental conditions for real-time decision-making criteria on water and nutrient runoff, predictions from forecasts, in-situ measurements and modelling routines need to be verified and improved (Klug & Kmoch, 2015). A higher quality of these predictions requires knowledge about near-surface hydro-geological structures to enable three-dimensional flow process modelling. Electrical

resistivity tomography (ERT) is one frequently applied technique to gather information about the often subtly heterogeneous subsurface geology and its properties (Aizebeokhai, 2010). Due to the three-dimensionality of geological structures, Badmus et al. (2011) point out that classical one-dimensional or two-dimensional survey designs are inappropriate to model structures below the surface. Consequently, Loke (2001) indicates that a three-dimensional resistivity survey, which uses a three-dimensional interpretation model, could deliver accurate subsurface information. In addition to pure geological tasks, 3D electrical resistivity tomography (3D ERT) has been applied in fields such as geophysical engineering and environmental geology (Kneisel et al., 2014).

For parallel located profile lines as used by Aizebeokhai & Singh (2013) and in order to generate high-quality 3D modelling, Aizebeokhai (2010) suggests the same distance for minimum electrode spacing and line spacing. However, inter-line spacing can be set at up to four times the electrode spacing in order to find a compromise between a reduction of working time and high data quality. Bentley & Gharibi (2004) additionally measured orthogonal linear 2D ERT profile lines for 3D model generation. Orthogonal sets of 2D profile lines were also added to a survey raster by Aizebeokhai et al. (2010).

According to Hauck & Kneisel (2008), Wenner electrode configuration has advantages in detecting horizontal structures of the subsurface which change with increasing depth. The smaller numbers of measurements taken compared to a Schlumberger array reduces data collection time. As stated by Schrott & Sass (2008), a Wenner array offers a good signal-to-noise ratio. Kneisel et al. (2014) summarize the Wenner configuration as presenting a good trade-off between high quality results and acceptable data acquisition time.

In this study, we apply ERT measurements to characterize a small slope with high water saturation and spring water release during storm events in Koppl (Figure 1). The main objective is to identify aquifers and aquicludes. We surmise that the slope springs crop out at an inclining impermeable subsurface layer, releasing the headwater. Furthermore, we hypothesize a small permeable subsurface layer, which is quick to become saturated during storm events and thus increases water flows.

2 Methods, Material and Software

Study Area

The precise subject of this study is the Koppl catchment (6 km2). Located in the south-west of the Mondsee catchment (248 km2), it is right on the Alpine/pre-Alpine border. Three major geological-tectonic units are present. The base comprises the marls of the Helvetic zone. The Northern Calcareous Alps consist of the Bajuvarikum and Tirolikum, which are thrust over the mudstones and sandstones of the Flysch zone (Tichy, 2000). The hilly landscape was shaped during the Würm ice age (10,000 years ago). The Salzach glacier consisted of several branches, of which the Guggenthal and Wiestal branches reunited in Koppl, after being separated by mount Gaisberg (1,288 m a.s.l) (Meneweger, 1993). The load of the Salzach glacier resulted in the compaction of silt and mudstones (Tichy, 2000). In the western part of Koppl, drainage was blocked during the last ice age. This resulted in the

genesis of blocked valley lakes and the deposition of banded clay. The impermeable sediments, silts and till from the Riß ice age (128,000 years ago) played a major role for the genesis of the raised bogs in Koppl (Meneweger, 1993).

A very dense river system of about 2 km/km² and a total of 490 km of rivers and ditches are characteristic of the Mondsee catchment. Together with the surrounding steep slopes and heavy soils, they explain fast runoff during extreme weather events, putting villages like Thalgau or St. Lorenz along Plainfelderbach and Fuschlerache at risk of being flooded (Klug & Oana, 2015). Rapid water collection is seen especially at the local fire station between Eisenstraße 7 and 11 in Koppl, our case study on the north-exposed slope. The geological map suggests a glacial formation of the slope (Egger & van Husen, 2003), where water is released mainly from one 'semi-captured' spring.

Electrical Resistivity Tomography

Uhlenbrook & Wenninger (2006) observed two hillslope/spring systems and found ERT to be an appropriate method to identify the various runoff components and flow pathways. To differentiate between the aquifer layer (water-bearing layer) and the aquiclude (impermeable layer), 2D electrical resistivity was applied using a constant current penetrating into the ground (Chambers et al., 2011). Four electrodes are involved within each resistivity measurement. Electrodes A and B feed the direct current into the subsurface. Based on this electrical flux I, an electrical field is built up in the subsurface (Schrott & Sass, 2008). This fundamental principle of geophysical measurement is the result of different natural materials like rocks, sediments and soils having different electrical resistivity values. The M and N electrodes measure the differences in electrical resistivity in the subsurface. The results are shown in voltage differences ΔV (Hauck & Kneisel, 2008). Based on current (I) and the resulting voltage difference, resistivity value ϱ is determined using the following equation:

$$\rho_a = K\frac{\Delta V}{I} \quad (1)$$

Equation 1: Electrical resistivity in the subsurface

K describes the so-called geometric factor, which is defined by the specific location of the active and potential electrodes of each measurement. The resulting ϱa is the apparent resistivity. As described by Hauck & Kneisel (2008), the true resistivity values can be derived by applying data inversion methods.

Data acquisition

For 2D electrical resistivity data collection, GeoTom MK-RES/IP/SP by Geolog 2000 was used. The measurement software used was GeoTom V724. The survey was conducted by arranging electrodes in parallel profile lines. The spacing between measurement lines was 6m. The two most southerly ERT lines represent an exception. Due to the course of the road, spacing had to be reduced to 5m. This measurement setup differs from the finer raster layout originally planned because of various challenges, including technical difficulties with the ERT device, bad weather conditions, and ongoing grassland cultivation processes, which resulted

in less measurement time than planned. Property lines in combination with grassland cultivation allowed measurements with 23 instead of 25 electrodes. The electrode spacing was therefore set to 4m. This spacing offers ERT profiles of 88m in length. The interpolation of missing electrodes was tested but omitted as they reduced the quality of the final model.

As shown in Figure 1, 26 2D parallel ERT profile lines were placed across the slope, with profile 1 in the south. Measurements were conducted using the Wenner electrode configuration. Since the ERT measurements could not be performed on one single day, we carried out our field work on 19 April and 11/12 May 2016. In order to determine possible deviations of data between April and May, a repetition of ERT profile line 11 was conducted.

Topographic data was collected using DGPS. The altitudes and coordinates of the starting and end points of the ERT profile lines were measured. This process was also performed for three springs. Further height information for points along the profile lines were extracted from a 1m resolution LiDAR digital elevation model (DEM). Before data inversion, GeoTom software was used to transfer topography information for each ERT measurement into a DAT-file.

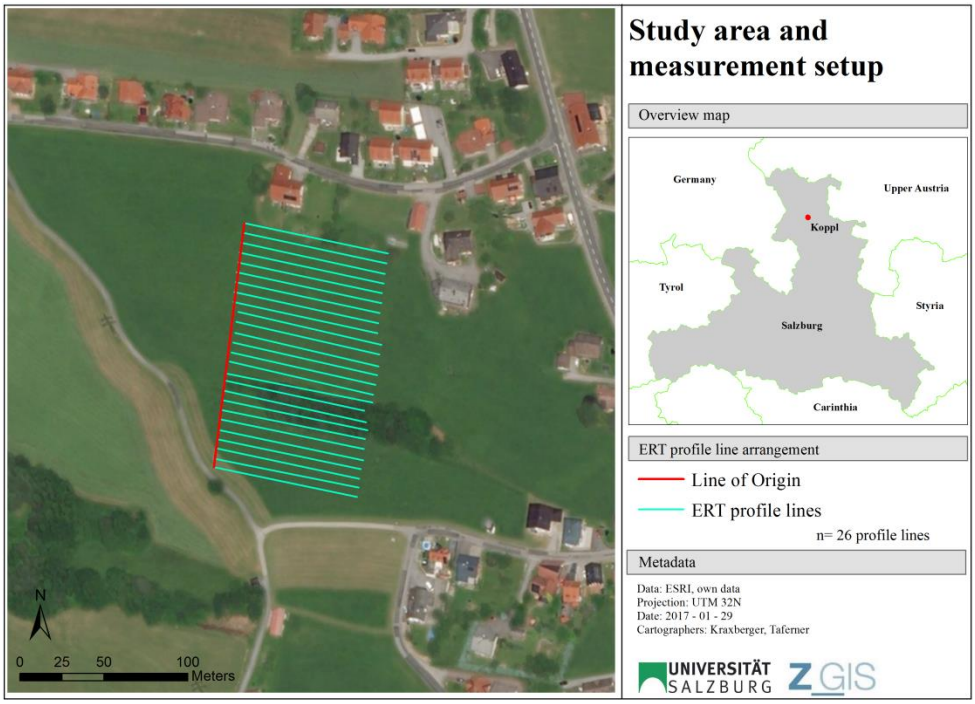

Figure 1: ERT profile line setup

Data inversion

All 2D ERT profiles collected were inverted separately using smoothness-constrained least-squares inversion in Res2DInv software. This enables a proof of quality for each single dataset. Prerequisite for 3D inversion is the collation of non-inverted 2D ERT profiles to a single 3D DAT file. As for the 2D inversion, the least-squares inversion method was also used for the 3D inversion. This divides the subsurface into rectangular prisms. We determined resistivity values for each generated prism, resulting in a minimal difference between calculated and measured apparent resistivity values. The quality of this minimization is expressed as root mean square (RMS) error value (Loke, 2008).

Data visualization

3D data visualization was performed using Paraview software (v5.0.1) to generate products such as slices and threshold graphics of resistivity using appropriate colour schemes. Coincidences between the subsurface and a surface runoff model created using the ArcGIS 10.3 hydrology toolbox were analysed based on the LiDAR model. The uppermost layer of the subsurface model was exported from Paraview to ArcGIS and georeferenced using DGPS measurements of the ERT profile lines. The perspective visualization of results was executed in ArcScene.

3 Results

Figure 2 shows the 3D subsurface model of the study area. The extent of the model is 149m from north to south and 88m from west to east. The penetration depth of the ERT measurements is 18m. The RMS errors between measured and apparent resistivity after five inversion iterations was 2.64%, which was then chosen for analysis. Resistivity values after inversion in Res3DInvx64 (v3.11.07) ranged from 10 to 1132 Ωm (shown in Figure 2). Low resistivity values (10–100 Ωm) are observed in the uppermost three vertical metres north and south of the coppice belt. Within this surficial layer, a series of elongated features are formed by cells of very low resistivity. These emerge downhill mainly from the eastern part of the model north of the coppice. Further bodies of low resistivity are located at a greater depth, of around 10m. This applies especially to central and western sections of the slope, south of the coppice. Comparable deep-seated bodies of low resistivity are found below 9m in the central parts, south of the coppice.

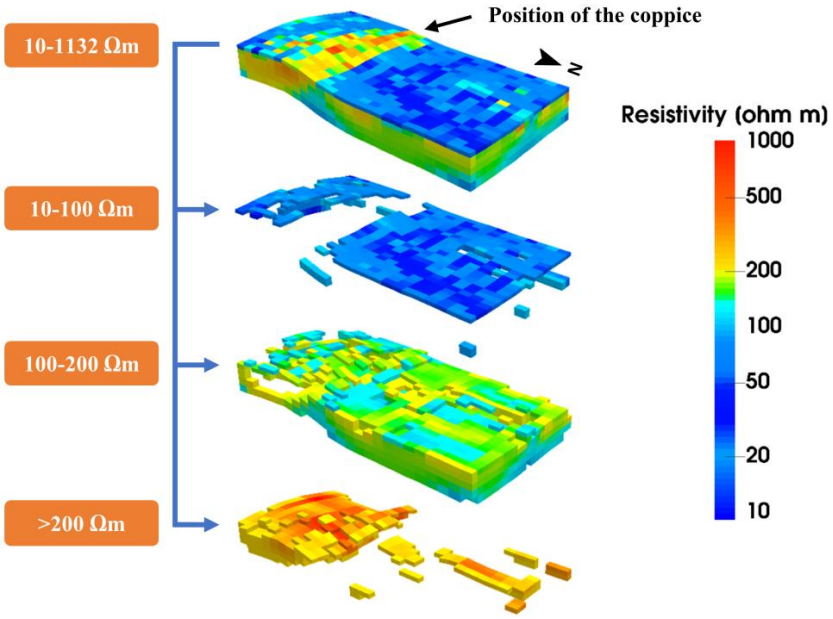

Figure 2: Partitioning of the 3D subsurface model

The westernmost segments south of the coppice do not show electrical resistivity values greater than 200 Ωm. Highest surficial resistivity north of the coppice is concentrated in a small knoll. Beneath the surficial zones of low resistivity are areas with material of 100-200 Ωm resistivity, which form the largest part of the model. The areas with the highest resistivity values (>200 Ωm) are concentrated on the steepest parts of the slope. This section is covered with trees. A few isolated building blocks of the model with electrical resistivity values of more than 200 Ωm are located downslope.

Any significant differences could be detected by a simple visual comparison of the 2D images generated by repeating the measurements of two ERT profiles. Resistivity values as well as their distribution showed only slight deviations.

4 Discussion

Similar to those of Kneisel et al. (2014), the results of the present study show that 3D ERT can help to detect heterogeneities such as moisture in small-scale areas. Despite a relatively low RMS error, the interpretation of results shown above is ambiguous. The reason for this is the lack of precision in ERT data analysis. As indicated by Beblo (1997) and Knödel et al. (2005), a material can be characterised by a range of resistivity values. Figure. 3 shows that these ranges might overlap. This challenge is present in every study which applies ERT as its single method and lacks validation data to enable a precise allocation of resistivity values to subsurface material.

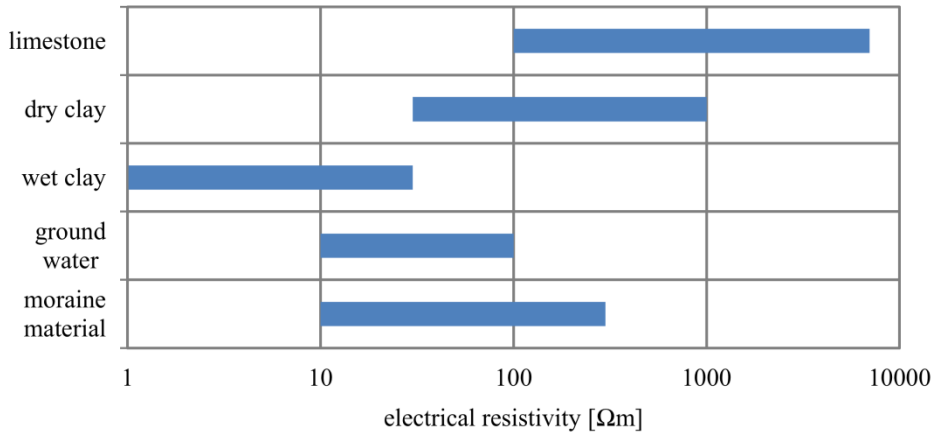

Figure 3: Electrical resistivity values of various materials. After Beblo (1997) and Knödel et al. (2005)

Based on the values in Figure 3, the large areas with low resistivity values (10–100 Ωm) north and south of the coppice are interpreted as water and water-saturated material. These layers represent aquifers. Cross sections in Figure 4 show their positions in the uppermost few metres of the subsurface. Surface runoff is assumed to be mainly responsible for this result. Following Aizebeokhai & Singh (2013), increased salinity due to fertilization of meadows could help explain high conductivity material at the surface.

Traces of notably low resistivity south of the coppice might relate to flow paths of outcropping springs. The same flow paths could also explain the elongated bodies of low resistivity at greater depth.

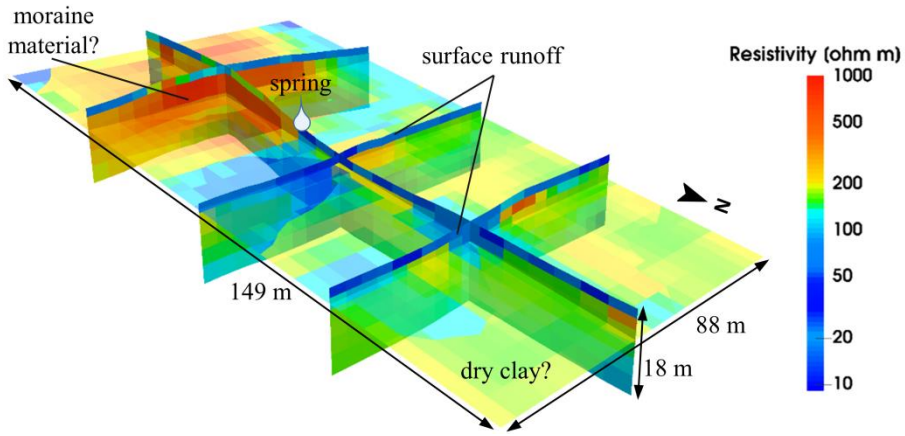

Figure 4: Slices through subsurface model

Figure 5 provides evidence for connections between low electrical resistivity values in the uppermost layer of the model and surface runoff. Outcrops of springs and concentrations of streams from runoff modelling show partial congruencies. Runoff modelling reveals that a

potential aquiclude crops out at the spring location. In case of precipitation and water infiltration, interflow processes transport the water back to the surface. Generally, the eastern runoff structures appear wetter than the western ones because the latter show extensively lower resistivity values. This might provide an indication of process differences, e.g. the drying-up speed after rainfall or snowmelt. Topographical structures such as hills show neither surface runoff nor extremely low resistivity values.

Material with electrical resistivity of 200–300 Ωm is interpreted as moraine material from the Salzach glacier. This assumption relies on empirical values as well as on geological information provided in section **Fehler! Verweisquelle konnte nicht gefunden werden.**. Furthermore, this moraine material acts as an aquiclude. Highest resistivity values (>300 Ωm) can be traced back to boulders most likely transported and deposited by the Salzach glacier. Material with 100–200 Ωm might be compacted dry clay from the last ice age.

A further point that influences the interpretation of results is variations in measurement conditions on the days of data acquisition. Precipitation in particular is a potential factor to be taken into account. As the first and second iterations of the repeated measurement showed similar electrical resistivity values and distribution, we believe that it would be appropriate to include ERT data from three different days in the one model.

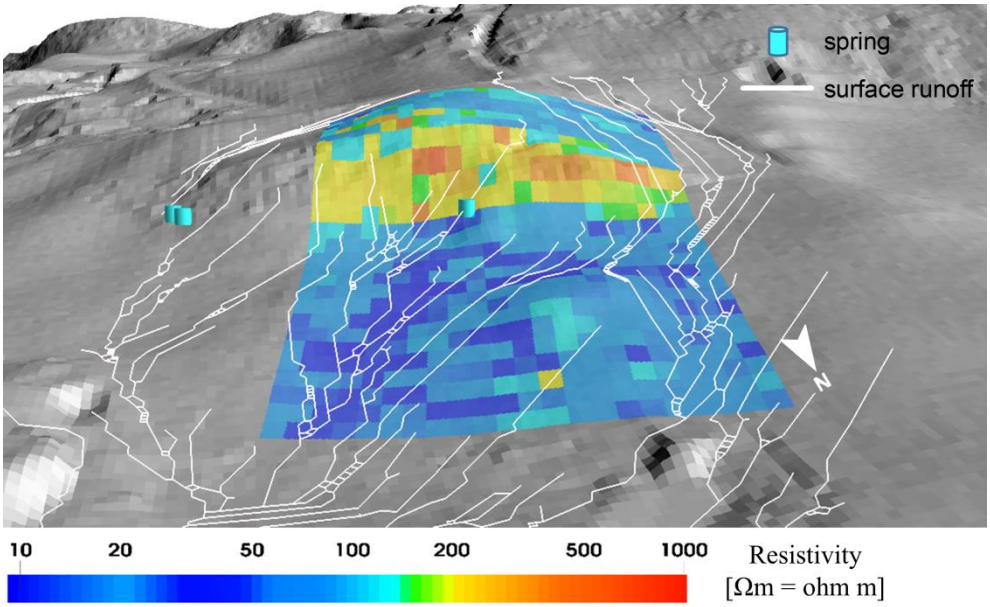

Figure 5*:* Runoff overlay and surface resistivity

5 Conclusion and Outlook

Application of ERT with the chosen measurement setup resulted in a meaningful three-dimensional model of the near subsurface. We pinpointed runoff concentration in the uppermost three metres north and south of the coppice as being the consequence of aquicludes. Material with high electrical resistivity represents moraine material as described in the literature. GPS measurements and runoff modelling in combination with ERT revealed lowest resistivity near springs and flow paths. Thus, our expectation of finding evidence of springs in the ERT profile was fulfilled. The understanding gained from this study can help to take measures such as the creation of drainage systems to prevent water damage to existing buildings and future construction projects. However, the results for the analysis of deeper layers cannot be proven without direct investigation of the shallow subsurface. For instance, core drillings using the calibration measurements for ERT equipment in the study could be used as supplemental confidence material (Kneisel et al., 2014). Future projects could comprise long-term studies of the same slope, which would allow variations of the electrical resistivity dependent on seasons or weather conditions to be detected. Additionally, trials focusing on tracer substances in runoff could be used to confirm assumptions regarding the emergence of headwater through the spring. Furthermore, an extension of the area surveyed could be performed by lengthening the ERT profile lines. This setup would also increase the penetration depth of the measurements. Following suggestions made by Loke (2001), the accuracy of the model could be increased by adding angular ERT measurements to the parallel profile lines. A 3D model with a higher resolution, involving narrower electrode and line spacing, could also provide further evidence about hydrogeological mechanisms. Finally, similar investigations close to the present study area would enhance knowledge of states, processes, structures and flows of water and nutrients in this particular part of the Mondsee catchment.

Acknowledgements

We would like to acknowledge the parcel owners for enabling our measurements. In addition, we thank the Geomorphology research group from the Department of Geography and Geology at the University of Salzburg for providing equipment and software.

References

Aizebeokhai, A. P. (2010). 2D and 3D geoelectrical resistivity imaging: Theory and field design. Scientific Research and Essays, 5(23), 3592-3605.

Aizebeokhai, A. P., Olayinka, A., & Singh, V. S. (2010). Application of 2D and 3D geoelectrical resistivity imaging for engineering site investigation in a crystalline basement terrain, southwestern Nigeria. Environmental Earth Sciences, 61(7), 1481-1492.

Aizebeokhai, A. P., & Singh, V. S. (2013). Field evaluation of 3D geo-electrical resistivity imaging for environmental and engineering studies using parallel 2D profiles. Current Science, 105(4), 504-512.

Badmus, B., Akinyemi, O., Olowofela, J., & Folarin, G. (2011). 3D electrical resistivity tomography (ERT) survey of a typical basement complex terrain. Journal of Emerging Trends in Engineering and Applied Sciences (JETEAS), 2(4), 680-686.

Beblo, M. (1997). Umweltgeophysik. Berlin: Ernst.

Bentley, L. R., & Gharibi, M. (2004). Two-and three-dimensional electrical resistivity imaging at a heterogeneous remediation site. Geophysics, 69(3), 674-680.

Chambers, J., Wilkinson, P., Kuras, O., Ford, J., Gunn, D., Meldrum, P., Pennington, C., Weller, A., Hobbs, P., & Ogilvy, R. (2011). Three-dimensional geophysical anatomy of an active landslide in Lias Group mudrocks, Cleveland Basin, UK. Geomorphology, 125(4), 472-484.

Egger, H., & van Husen, D. (2003). Geologische Karte der Republik Österreich 1:50000. Blatt 64 Straßwalchen. Verl. der Geol.-BA., 1.

Hauck, C., & Kneisel, C. (2008). Electrical methods (chapter 1). In C. Hauck & C. Kneisel (Eds.), Applied Geophysics in periglacial environments. Cambridge: Cambridge University Press.

Hofstätter, M., Matulla, C., Wang, J., & Wagner, S. (2010). PRISK-CHANGE Veränderung des Risikos extremer Niederschlagsereignisse als Folge des Klimawandels. Abschlussbericht der Fachabteilung Klimavariabilität/Modellierung in der Abteilung Klimaforschung. ZAMG, Vienna.

Klug, H., & Kmoch, A. (2015). Operationalizing environmental indicators for real time multi-purpose decision making and action support. Ecological Modelling, 295, 66-74. doi: http://dx.doi.org/10.1016/j.ecolmodel.2014.04.009

Klug, H., Kmoch, A., & Reichel, S. (2015). Adjusting the Frequency of Automated Phosphorus Measurements to Environmental Conditions. Journal for Applied Geoinformatics, GI_Forum 2015, 1, 592-601. doi: http://dx.doi.org/10.1553/giscience2015s592

Klug, H., & Oana, L. (2015). A Multi-purpose Weather Forecast Model for the Mondsee Catchment. GI_Forum, 2015, 600-609. doi: http://dx.doi.org/10.1553/giscience2015s602

Kneisel, C., Emmert, A., & Kästl, J. (2014). Application of 3D electrical resistivity imaging for mapping frozen ground conditions exemplified by three case studies. Geomorphology, 210, 71-82.

Knödel, K., Krummel, H., & Lange, G. (2005). Handbuch zur Erkundung des Untergrundes von Deponien, Band 3: Geophysik. Berlin Heidelberg: Springer.

Loke, M. (2001). Tutorial: 2D and 3D electrical imaging surveys. Unpublished course notes. Penang, Malaysia.

Loke, M. (2008). RES2DINV version 3.54-Rapid 2D resistivity and IP inversion using the least-squares method: Geoelectrical Imaging 2-D and 3-D (pp. 130). Malaysia: Geotomo Software.

Meneweger, H. (1993). Zur quartären Entwicklung des Gebietes um Koppl - Ebenau - Faistenau. Unpublished diploma thesis, Department of Geology, University of Salzburg, 111.

Schrott, L., & Sass, O. (2008). Application of field geophysics in geomorphology: advances and limitations exemplified by case studies. Geomorphology, 93(1), 55-73. doi: http://doi.org/10.1016/j.geomorph.2006.12.024

Swierczynski, T., Brauer, A., Lauterbach, S., Martín-Puertas, C., Dulski, P., von Grafenstein, U., & Rohr, C. (2012). A 1600 yr seasonally resolved record of decadal-scale flood variability from the Austrian Pre-Alps. Geology, 40(11), 1047-1050.

Swierczynski, T., Lauterbach, S., Dulski, P., Delgado, J., Merz, B., & Brauer, A. (2013). Mid-to late Holocene flood frequency changes in the northeastern Alps as recorded in varved sediments of Lake Mondsee (Upper Austria). Quaternary Science Reviews, 80, 78-90. doi: http://dx.doi.org/10.1016/j.quascirev.2013.08.018

Tichy, G. (2000). Die Geologie von Koppl. Eine kleine Gemeinde aber reich an Besonderheiten. In M. Bahngruber, H. Paarhammer & F. Zaisberger (Eds.), Heimat Koppl: Chronik der Gemeinde. Koppl: Eigenverlag der Gemeinde Koppl.

Uhlenbrook, S., & Wenninger, J. (2006). Identification of flow pathways along hillslopes using electrical resistivity tomography (ERT). Predictions in ungauged basins: promise and progress, 303, 15-20.